Cement and Concrete Research 42 (2012) 158–165

Contents lists available at SciVerse ScienceDirect

Cement and Concrete Research

journal homepage: http://ees.elsevier.com/CEMCON/default.asp

Thermodynamic modeling of solid solutions between monosulfate and monochromate $3CaO \cdot Al_2O_3 \cdot Ca[(CrO_4)_x(SO_4)_{1-x}] \cdot nH_2O$

Sabine M. Leisinger [a,b,*], Barbara Lothenbach [c], Gwenn Le Saout [c], C. Annette Johnson [a]

[a] Eawag, Swiss Federal Institute of Aquatic Science and Technology, Ueberlandstrasse 133, CH-8600 Duebendorf, Switzerland
[b] Institute of Biogeochemistry and Pollutant Dynamics, ETH, CH-8092 Zurich, Switzerland
[c] Empa, Swiss Federal Laboratories for Concrete and Construction Chemistry, Ueberlandstrasse 129, CH-8600 Duebendorf, Switzerland

ARTICLE INFO

Article history:
Received 9 November 2010
Accepted 15 September 2011

Keywords:
Characterization (B)
Thermodynamic calculations (B)
X-Ray Diffraction (B)
Chromium (D)
Monosulfate (D)

ABSTRACT

In hydrated cement paste AFm-phases are regarded to play an important role in the binding of the toxic contaminant chromate through isomorphic substitution with sulfate. Solid solutions formation can lower the solubility of the solids, thus reducing chromate leaching concentrations.
Solid solutions between monosulfate and monochromate were synthesized and characterized by X-ray diffraction (XRD), thermogravimetric analysis (TGA), scanning electron microscopy (SEM), energy dispersive x-ray spectroscopy (EDX) and inductive coupled plasma optical emission spectroscopy (ICP-OES). Based on the measured ion concentrations in solution total solubility products of the solid solution series were determined. For pure monochromate a $\log K = -28.4 \pm 0.7$ was determined. Results from solid and solution analysis showed that limited solid solutions exist. Based on XRD diffractograms a solid solution with a miscibility gap $0.15 < Crx < 0.85$ with a dimensionless Guggenheim parameter of 2.43 was proposed.

1. Introduction

Chromium is a common contaminant in chromate ore processing wastes or wastes from stainless steel production. Chromium, mostly in the form of the trivalent Cr(III) cation, is present also in the earth crust and thus in different cementitious materials such as Portland cement, slag or fly ash. Cr(III) can substitute for Al in most calcium aluminate hydrate phases or precipitate as chromium hydroxide, $Cr(OH)_3$ [1]. Oxidizing conditions and high temperatures as present during clinker manufacturing lead to an oxidation of Cr(III) to Cr(VI), chromate. Ordinary Portland cements (OPC) contain approximately 60 ppm chromate from geogenic sources [2]. Chromate is toxic, in alkaline environment present as oxyanion (CrO_4^{2-}), well soluble and poses thus a significant leaching potential [3,4] and due to its high toxicity a health risk [3].

For the immobilization of the highly mobile chromate, incorporation into mineral phases becomes the relevant binding mechanism. Among others, AFt- and AFm-minerals have a high anion immobilization potential due to their structures and due to the ease of formation from a wide range of starting materials [5–8]. AFt is shorthand for Alumino-Ferrite-tri phases like ettringite $3CaO \cdot Al_2O_3 \cdot 3CaSO_4 \cdot 32H_2O$ whereas AFm stands for Alumino-Ferrite-mono phases such as monosulfate $3CaO \cdot Al_2O_3 \cdot CaSO_4 \cdot 12H_2O$. The identical charge and comparable radii of SO_4^{2-} and CrO_4^{2-} ions (2.3 Å and 2.4 Å respectively [9]) suggest that chromate should readily substitute in the crystal structure of ettringite and monosulfate to form solid solutions [10]. The formation of solid solutions can lower the solubility of the solids, thus reducing chromate leaching concentrations. The solid solutions between CrO_4-and SO_4 ettringite has been previously investigated [11] but no data are available concerning the possible solid solution formation between CrO_4- and SO_4-AFm. AFm phases belong to the double layered hydroxide family (LDH) and consist of a layered crystal structure built by periodical stacking of positively charged $[Ca_2Al(OH)_6\ 2H_2O]^+$ octahedral layers and negatively charged interlayers consisting of anions and water molecules. The structure of the end member SO_4-AFm has been described by Allmann [12]. Two structures have been proposed for the end member CrO_4-AFm by Segni [13] and Rapin [14]. The layer staking and arrangement of the anions in the interlayer lead to symmetry *R* 3 for SO_4-AFm and *P* 3 for CrO_4-Afm. The size of the CrO_4^{2-} (distances Cr-O around 1.69 Å in [13] and 1.88 Å in [14]) anion is larger than of the SO_4^{2-} (S-O distances from 1.42 to 1.46 Å) leading to an increase of the number of layer in the repeating unit (from 2R to 3R). The SO_4^{2-} tetrahedral anion, located in the middle of the interlayer, has a pyramidal configuration with the three oxygen atoms closed to the hydroxyl groups in the brucite-like layer and the fourth one pointing toward the opposite hydroxide plane. In the case of the CrO_4^{2-} anion, the configuration is similar in the structure described by Rapin [14], but, in the

* Corresponding author at: Eawag, Swiss Federal Institute of Aquatic Science and Technology, Dep. of Waterresources and Drinking Water, Ueberlandstrasse 133, CH-8600 Duebendorf, Switzerland. Tel.: +41 44 823 5362.
E-mail address: sabine.leisinger@eawag.ch (S.M. Leisinger).

0008-8846/$ – see front matter
doi:10.1016/j.cemconres.2011.09.005

structure proposed by Segni [13] the seventh coordination position of the Ca atoms is occupied statistically either by a water molecule or the fourth oxygen of the CrO_4^{2-} anion. The structure can be described by a stacking of two kinds of layer, one negatively charged $[Ca_2Al(OH)_6\ CrO_4\ H_2O]^-$ and the other positively charged $[Ca_2Al(OH)_6\ 2H_2O]^+$ plus interlayer free water molecules [15]. This grafting reaction in which a water molecule bonded to Ca is replaced by the oxygen of the interlayer anion has also been observed in other AFm structures as CO_3-AFm [16] and NO_3-AFm [17] and may explain why solid solution have been observed between OH and SO_4-AFm while between SO_4 and CO_3 –AFm no solid solution are formed [18]. However, recent studies show multiple and complex scenarios in bi anionic AFm. For examples, in (Cl, CO_3)-AFm, a solid solution has been observed where chloride and carbonate anions are located on the same crystallographic site in the interlayer with statistical disorder [19,20]. No grafting reaction is observed in this bi anionic compound whereas in the CO_3-AFm grafting reaction occurs [16]. In the (Cl, SO_4)-AFm, Kuzel's salt $3CaO\ Al_2O_3\ 1/2CaSO_4\ 1/2CaCl_2\ 11H_2O$ is a two-stage layered compound with two distinct interlayers, which are alternatively filled by Cl and by SO_4 with no grafting [21]. According to Mesbah et al. [21], the staging feature of the Kuzel's salt and the different charge of the anion may explain the difficulties to substitute chloride and sulphate in (Cl, SO_4)-AFm.

In this study, we have investigated the solid solution between CrO_4-AFm and SO_4-AFm as for the prediction of long-term chromate leaching potential, the knowledge of the solid solution formation and its stabilising influence are crucial.

2. Experimental

2.2. Materials

All chemicals were at least of pro analysis (p.a.) grade; $CaCrO_4$, $CaCO_3$, $CaSO_4•2H_2O$ and Al_2O_3- powder, KOH solution (1 M, Titrisol), HNO_3 Suprapur 65%, ICP-OES multi-elements standard solution IV and SO_4-anion standard solution were used.

All handling of material, sampling and pH measurements were carried out in a glovebox (Mecaplex) equipped with a CO_2 scrubber (pCO_2<1 ppm, DMP Ltd., Switzerland) to prevent possible CO_2 contamination. Ultrapure water (resistivity >18 MΩ.cm) was used for the preparation of solutions and rinsing processes. All polyethylene bottles, tubes and glassware were leached in acid solutions (0.3 M HCl, Merck) for at least 24 h and rinsed three times with ultrapure water.

2.3. Synthesis of solid phases

2.3.1. End members: pure SO_4- and CrO_4-AFm

Pure monochromate $3CaO•Al_2O_3•CaCrO_4•nH_2O$ was synthesized in triplicate in precipitation experiments at varying pH values from 11 to 14 (n stands for the different possible hydration states). Stoichiometric amounts of freshly burned tricalcium aluminate clinker (C_3A) (4 mmol), and $CaCrO_4$ (4 mmol) were added to 0.001 M – 1 M KOH solution (50 ml). C_3A was prepared by burning $CaCO_3$ and Al_2O_3 at 1450 °C for 24 hours [22]. The liquid/solid ratio was held constant at 20. The mixtures were equilibrated for 3 months in sealed HDPE bottles (50 ml) at 25 °C on a rotary shaker at 125 rpm. The samples were then centrifuged for 20 min at 4000 rpm. An aliquot of the supernatant (6 ml) was directly used for the measurement of pH and the rest was filtered through 0.45 μm nylon membrane filters (Titan), and acidified with concentrated HNO_3 Suprapur at a ratio of acid:water equal to 1:100 for ICP-OES.

Synthesis of pure monosulfate $3CaO•Al_2O_3•CaSO_4•nH_2O$ was only carried out at a pH of 11. Experimental setup and procedure was accordingly to the synthesis of pure monochromate. The solid residues were washed with acetone, dried and stored in desiccators over silica gel (H_2O absorbent) and soda lime (CO_2 absorbent).

2.3.2. Solid solutions between monosulfate and monochromate

The mixed phases of the series were synthesized according to the following precipitation reaction:

$$C_3A + xCaCrO_4 + (1-x)CaSO_4 \cdot 2H_2O + (10+2x)H_2O = Ca_4\left[Al(OH)_6\right]_2(CrO_4)_x(SO_4)_{1-x} \cdot 6H_2O \quad (1)$$

Stoichiometric amounts of freshly burned C_3A (4 mmol), $CaCrO_4$ and/or $CaSO_4•2H_2O$ (totally 4 mmol) were mixed with 0.001 M KOH solution (50 ml) to obtain different total chromate mole fractions ($XCrO_{4,\ TOT} = [CrO_4^{2-}]\ /\ ([CrO_4^{2-}]+[SO_4^{2-}] = 0,\ 0.1,\ 0.2,\ 0.4,\ 0.6,\ 0.8$ and 1). While $XCrO_{4,\ TOT}$ represents total chromate mole fractions added to the system, x is the chromate mole fraction of the solids that precipitated. Samples are named Crx such as Cr0 for pure monosulfate $3CaO•Al_2O_3•CaSO_4•12H_2O$ and Cr1 for pure monochromate $3CaO•Al_2O_3•CaCrO_4•12H_2O$.

Since equilibration of solid solutions may take longer than for pure phases [23], the mixtures were stored for 6 month. Then the solid residues were also washed with acetone, dried and stored in desiccators over silica gel (H_2O absorbent) and soda lime (CO_2 absorbent).

2.4. Characterization of the solid phases

After drying, the samples were ground by hand with an agate mortar to <63 μm and analyzed by X-ray diffraction (XRD), thermogravimetric analysis (TGA), scanning electron microscopy (SEM), energy dispersive x-ray spectroscopy (EDX) and inductive coupled plasma optical emission spectroscopy (ICP-OES).

SEM was used to control the morphology of the solid phases. The measurements were done with a Nova Nano SEM 230 FEI at high vacuum mode. Solid stoichiometry was determined using ICP-OES. 0.1 g of a solid sample was dissolved in 500 μl HNO_3 Suprapur in a 50 ml HDPE bottle and filled with ultrapure water to 50 ml. Samples were diluted 1:10 and 1:100 prior to measurement. TGA was carried out on a TGA/SDTA 851 apparatus by Mettler Toledo. The samples (8–12 mg) were heated under N_2 over a temperature range of 30–980 °C at a rate of 20 °C/min. TGA was carried out to observe mass changes in relation to changes in temperature and time. The determined mass losses were used to determine the water content of the solids and to estimate fractions of the solid that was CO_2. Measurements were carried out in triplicate. The purity, crystallinity and the solid solution examination of the products were analyzed by X-ray diffraction (XRD) using a PANalytical X'Pert PRO XRD system with CuKα radiation. Elemental silicon was mixed to the powder samples as internal standard for the determination of the unit cell parameters. The evaluation software X'Pert HighScore Plus was used for phase identification and solid solution examinations. The unit cell parameters for monosulfate were determined using Rietveld refinement of the structure proposed by Allmann et al. [12] and for monochromate a Le Bail fit was carried out [24]. At 98% rh, the unit cell parameters of the monochromate phase deduced by a Le Bail fit a = 5.74 Å and c = 30.72 Å (interlayer distance 10.2 Å) correspond well to those given by Feitknecht and Buser [25] (a = 5.75 Å and interlayer distance 10.0 Å), Göske et al. [26] (a = 5.75 Å and c = 30.73 Å, interlayer distance 10.2 Å, PDF file 00-052-0654), Rapin [14] (a = 5.75 Å and c = 19.42 Å, interlayer distance 9.7 Å), and Segni [13] (a = 5.75 Å and c = 20.16 Å, interlayer distance 10.1 Å). Attempts to perform Rietveld analysis based on the structure proposed in Segni [13] and Rapin [14] were not successful. This difference may be explained by the existence of different positions of the CrO_4^{2-} anion in the interlayer depending on the way of synthesis. Unfortunately, strong preferred orientation and broad peaks of the pattern do not permit a structure refinement of our sample and to confirm or not the grafting of the anion.

To study the effect of relative humidity on AFm phases, a climatic chamber (Anton Paar THC) specially designed for the X-ray

diffractometer was used in order to control both temperature and relative humidity. The relative humidity was increased up to 98% and stabilized at a temperature of about 20 °C.

2.5. Characterization of the liquid phase

The pH measurement was carried out with an Aquatrode Plus, Pt 1000 electrode from Metrohm. Prior to the measurements the pH electrode was calibrated by titration with fresh KOH-solutions (0.001-1 M) to minimize the alkali error, i.e. the error in the pH measurements caused by the presence of high concentrations of alkalis such as potassium or sodium. Alkali ions interfere with the H^+ resulting in a measured pH value that is lower than the actual pH. The alkali error increases with increasing pH values, higher alkali concentrations and increasing temperatures. The voltage reading was correlated to the calculated target pH-value of the respective KOH-solution considering ionic strength as well as the measured temperature of the solution. Dissolved concentrations of Ca, Al, K, Cr and SO_4, were determined by ICP-OES according to the method described for solid phases. Charge balance errors of all samples were <10%.

2.6. Thermodynamic modeling

GEMS is a broad purpose geochemical modeling code. The principle of GEMS is the minimization of the Gibbs energy of a complex chemical system. It computes mass balances, based on equilibrium phase assemblages and speciation in a complex chemical system from its total bulk elemental composition. Chemical interactions involving solids, solid solutions, gas mixture and aqueous electrolyte are considered simultaneously [27]. A built-in thermodynamic database [28] is provided. This database can easy be extended and fitted to the user-defined projects. The thermodynamic data used are compiled in Table 1.

Activity coefficients of aqueous species y_i were then computed with the built-in expanded extended Debye-Hückel equation in Truesdell-Jones form (Eq. (2)).

$$\log \gamma_i = \frac{-A_y z_i^2 \sqrt{I}}{1 + B_y a_i \sqrt{I}} + b_y I \quad (2)$$

where z_i denotes the charge of species i, I the effective molal ionic strength, a_i is a parameter dependent on the size of ion i, b_y is a semi-empirical parameter (0.64 at 25 °C), and A_y and B_y are P,T-dependent Debye-Hückel solvent parameters. This activity correction should be applicable up to 1–2 m ionic strength [27,28]. The measured ion concentrations were used as input in GEMS for the calculation of the solubility product (log K). Based on the calculated ion activities (using the extended Debye-Hückel equation), the solubility products of pure CrO_4- and SO_4-AFm were calculated. All calculated solubility products were converted to zero ionic strength.

3. Experimental results and discussion

3.1. Solid analysis

3.1.1. SEM

The two pure phases, monosulfate and monochromate, exhibited a different morphology both in size and shape (Fig. 1 top left and top right). While pure monosulfate crystallized to a euhedral hexagonal platelets shape with diameters of around 20 μm, monochromate crystallites precipitated as subhedral platelets with a diameter around a few micrometers. Crystallites in the mixtures formed at different sizes and morphologies. Some crystallites showed clear hexagonal platelets corresponding to monosulfate, while at others only layered platelets without sharp borders were observed (Fig. 1, at the bottom). Samples looked as if they were a mechanical mixture of both end members SO_4- and CrO_4-AFm. Additionally, traces of

Table 1
Thermodynamic data used for speciation calculations.

Reaction		log K_{s0}	Ref.
Aqueous Species			
$H_2O = OH^- + H^+$		−14 .0	[28]
$K^+ + H_2O = KOH^0 + H^+$		−14.46	[28]
$Ca^{2+} + H_2O = CaOH^+ + H^+$		12.78	[28]
$Ca^{2+} + HCO_3^- = CaHCO_3^+$		1.11	[28]
$Ca^{2+} + HCO_3^- = CaCO_3 + H^+$		−7.11	[28]
$SO_4^{2-} + H^+ = HSO_4^-$		1.99	[28]
$Ca^{2+} + SO_4^{2-} = CaSO_4^0$		2.3	[28]
$K^+ + SO_4^{2-} = KSO_4^-$		0.85	[41]
$CrO_4^{2-} + 2H^+ = H_2CrO_4^0$		6.31	[42]
$CrO_4^{2-} + H^+ = HCrO_4^-$		6.55	[42]
$2CrO_4^{2-} + 2H^+ - H_2O = Cr_2O_7^{2-}$		4.7	[42]
$Ca^{2+} + CrO_4^{2-} = CaCrO_4^0$		2.77	[43]
$K^+ + CrO_4^{2-} = KCrO_4^-$		0.78	[41]
$Al^{3+} H_2O = AlOH^{2+} + H^+$		−4.96	[28]
$Al^{3+} + 2H_2O = Al(OH)^+_2 + 2H^+$		−10.59	[28]
$Al^{3+} + 3H_2O = Al(OH)_3^0 + 3H^+$		−16.43	[28]
$Al^{3+} + 4H_2O = Al(OH)_{4-} + 4H^+$		−22.88	[28]
$Al^{3+} + SO_4^{2-} = AlSO_4^+$		3.9	[28]
$Al^{3+} + 2SO_4^{2-} = Al(SO_4)_2^-$		5.9	[28]
Solid phases			
Portlandite	$Ca(OH)_2 + 2H^+ = Ca^{2+} + 2H_2O$ -	22.8	[28]
Gypsum	$CaSO_4 * 2H_2O = Ca^{2+} + SO_4 + 2H_2O$	−4.58	[28]
Calcite	$CaCO3(s) + H^+ = CaHCO^{3+}$	1.85	[28]
Al-hydroxide am.	$Al(OH)_{3,\ amph} + OH^- = Al(OH)_4^-$	0.24	[28]
calcium chromate	$CaCrO_4 = Ca^{2+} + CrO_4^{2-}$	−2.77	[44]
CrO_4-AFm	$Ca_4(Al(OH)_6)_2(SO_4)*6H_2O = 4Ca^{2+} + 2Al(OH)_4^- + SO_4^{2-} + 4OH^- + 6H_2O$	$-29.7\ _{+/-\ 04}$	this study
SO_4-AFm	$Ca_4(Al(OH)_6)_2(CrO_4)*6H_2O = 4Ca^{2+} + 2Al(OH)_4^- + CrO_4^{2-} + 4OH^- + 6H_2O$	$-28.4\ _{+/-0.7}$	this study

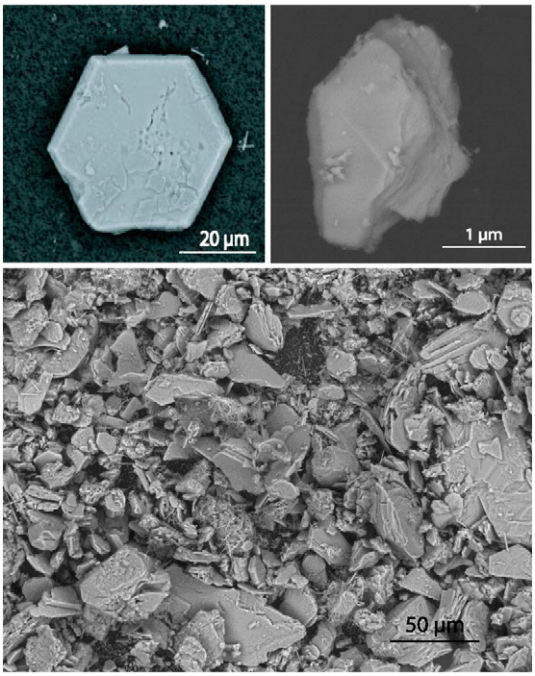

Fig. 1. SEM pictures showed pure SO_4-AFm (top left) and pure CrO_4-AFm (top right). The crystals of sample Cr0.5 varied both in size and shape (at the bottom). Traces of ettringite were observed especially in samples with increased Crx content.

ettringite-needles were observed in all samples. The amount of ettringite increased with x.

3.1.2. Chemical composition by ICP-OES

Measured chromate mole fractions of the solid (x) agreed with total chromate mole fractions ($XCrO_{4,\ TOT}$) of the prepared experiments for samples $0<XCrO_{4,TOT}<0.4$ (Table 2). At higher $XCrO_{4,\ TOT,}$ precipitated solids contained a lower x than expected. The chemical analyses give the composition of the bulk samples. However, as no other chromate of sulfate containing solids than the AFm-phases were detected (with exception of traces of ettringite in the pure and high sulfate samples), the bulk composition was assumed to correspond to the AFm-composition. The differences between the precipitated x in the solids and the $XCrO_{4,\ TOT}$ in the system is due to the around 10 times lower solubility product (~1 log unit) of pure SO_4-AFm ($\log K = -29.6$) compared to pure CrO_4-AFm ($\log K = -28.4$), see results below, indicating a higher stability of the SO_4-AFm. Thus the solid samples prepared at a higher $XCrO_{4,TOT}$ were more enriched in SO_4 than the corresponding solutions. This observation is comparable to the findings of other solid solution precipitation experiments [8,11]. In the present paper, all samples are labelled according to the precipitated x (nomenclature in the last column of Table 2).

Table 2
Results of solid digest analyses of synthesized $Ca_4(Al(OH)_6)_2(CrO_4)_x(SO_4)_{1-x}{\cdot}n\ H_2O$.

[a]$XCrO_{4,TOT}$	Ca	Al	CrO_4	SO_4	Ca	Al	CrO_4	SO_4	Crx
	mg/g solid				Normalized to 4 Ca				
0	261.5	103.7		210.0	4	2.4	0.0	1.3	0
0.1	248.2	101.5	10.4	180.0	4	2.4	0.1	1.2	0.1
0.2	230.1	94.3	18.7	150.0	4	2.4	0.3	1.1	0.2
0.4	242.9	99.0	41.2	125.0	4	2.4	0.5	0.9	0.4
0.6	250.0	103.3	60.9	95.0	4	2.4	0.7	0.6	0.5
0.8	247.2	101.3	75.3	85.0	4	2.4	0.9	0.6	0.6
1	231.9	92.3	108.9	0.0	4	2.4	1.4	0.0	1

[a] chromate mole fractions = $[CrO_4]/([CrO_4]+[SO_4])$ present in the system.
[b] chromate mole fraction of solids precipitated.

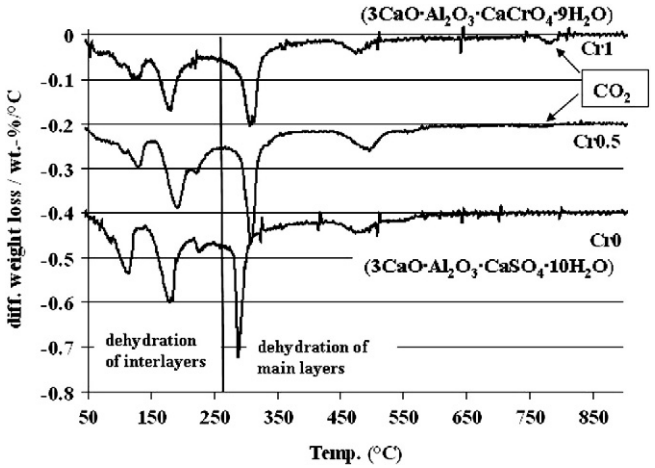

Fig. 2. DTGA measurements of monosulfate (Cr0) and monochromate (Cr1) and the solid solution sample (Cr0.5) showed the dehydration steps of the interlayers (50–250 °C) and the main weight loss of the main layers (at 290–300 °C). The dehydration of the main layer moved to higher temperatures for samples with higher Crx content. Traces of CO_2 ingress (~760 °C) is observed in Cr1 and the solid solution sample Cr0.5.

3.1.3. TGA

Thermogravimetric analysis showed that total mass lost of the samples with $0<x<0.5$ and dried over silica gel was between 30.4 - 30.8 weight %. This corresponds to a stable hydration state of 10 ± 0.4 water molecules per mole substance $3CaO\cdot Al_2O_3\cdot Ca[(SO_4)_{1-x},(CrO_4)_x]\cdot 10H_2O$. Pure CrO_4-AFm showed a smaller mass lost of 29.4 weight % corresponding to a hydration state of 9 ± 0.1 (Fig. 2). The dehydration behavior between 50 and 250 °C where the loosely bound water from the interlayer is lost, depends on the drying method which determines the hydration states of the samples; AFm phases may have several different water contents [29]. At a temperature higher than 250 °C water loss of the main layer is observed. An additional peak between 700–750 °C belongs to mass lost from volatile CO_2. However the CO_2 contaminations were very small (<1 weight %) and only observed in CrO_4-AFm and the sample Cr0.6.

3.1.4. XRD of pure CrO_4-AFm

First XRD analyses of pure CrO_4-AFm phases were carried out at increasing relative humidity (r.h.) (Fig. 3). Starting at an ambient r.h. of approximately 35% the peak (009) corresponded well to the CrO_4-AFm with a hydration state of 9 compared to the database file (PDF 00-042-0063) of the International Center for Diffraction Data (ICDD).

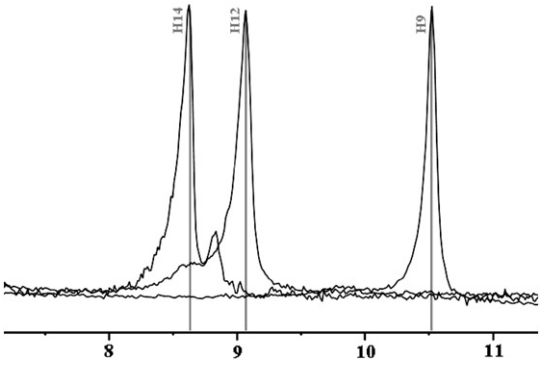

Fig. 3. Monochromate peak (003) from XRD measurements show the shifts to higher 2 Theta values with decreasing relative humidity (rh). Starting at 98% rh monochromate with a hydration state of 14 was observed (Cr14). At lower rh hydration states of 12 and 9 (ambient rh) are shown. Water uptake and release according to the humidity conditions was a reversible process and occurred within a few minutes. The following PDF files correspond to the grey lines: Cr14 to 00-052-0654, Cr12 to 00-041-0478 and Cr9 to 00-042-0063.

With increasing r.h. the peak shifted to lower 2θ values and hydration states of 12 and 14 could be identified (PDF files 00-041-0478 and 00-052-0654 respectively). These results are in good agreement with previous results [26,30–32]. When fully hydrated samples were subjected to lower humidity's, water molecules were released quickly released again and the peak shifted back to higher 2 θ values (Fig. 3). The peak shifting can be explained by the increased amount of water molecules present in the interlayers causing a swelling at high r.h. and the release of the water molecules from the interlayers resulting in a shrinking. This shows that SO_4- and CrO_4-AFm phases are extremely sensitive to relative humidity and that the process of water uptake and release is reversible.

3.1.5. XRD of mixed phases

Beside the several existing hydration states a peak shift occurs also through possible ion exchange with different ionic radius (Cr^{6+} = 0.4 Å, S^{6+} = 0.26 Å) [33]. The chromium radius is larger than the sulfur radius. Thus, with increasing $XCrO_4$ in the sample the more CrO_4 is present in the interlayer and the larger the interlayer distance becomes - causing a peak shift to lower 2 θ values.

The freshly prepared mixed samples were measured at ambient r.h. (~35). The diffractograms showed well crystallized phases (Fig. 4). The CrO_4-AFm end member correlated well to monochromate with $3CaO \cdot Al_2O_3 \cdot CaCrO_4 \cdot 9H_2O$ as illustrated above. For monosulfate dried at ambient r.h. a peak was observed at 2<theta>= 10.5° (d-spacings 8.42 Å). This corresponds to $3CaO \cdot Al_2O_3 \cdot CaSO_4 \cdot 10.5\ H_2O$ according to Pöllmann [29] and to $3CaO \cdot Al_2O_3 \cdot CaSO_4 \cdot 10H_2O$ according to Dosch [34].

The analysis of the solid solution series shows that clear peak shifting occurs except for sample Cr0.1 (Fig. 4). Starting at pure CrO_4-AFm the peak shifts more and more to higher 2<theta> values with decreasing Crx in the sample. Only in sample Cr0.1 the peak is not visible any more. Starting at the bottom at the SO_4-AFm end member the peak as well shifts with increasing $XCrO_4$ to lower 2<theta> values as expected. These peak shifts are due to the anion exchange between SO_4 and CrO_4 indicating that solid solution forms. However, since in all the samples (again except Cr0.1) we observe 2 distinct peaks instead of one, two mixed phases SO_4-CrO_4 AFm phases are present. One of these phases is mainly composed of CrO_4 while the other one mainly contains SO_4 anions. The presence of two peaks is not obvious in the sample Cr0.6. The small picture to the right of Fig. 4 reveals a small but not insignificant second peak close to the SO_4-AFm end member.

Due to the observed strong preferred orientation of the crystals, the quality of the peaks was too poor to carry out Rietveld refinements except for pure SO_4-AFm samples. Further investigations on better crystallized samples would be needed to investigate the influence of the positions of the anions in the interlayer on the ability to form solid solutions. Since the SO_4-AFm crystals were large (see Fig. 1) compared to mixed phases and pure CrO_4-AFm, there were enough counts for all peaks to carry out a Rietveld refinement. Unit cell parameters a and c of 5.76 Å and 26.86 Å were determined. For all other samples the d-spacing values are determined with a reasonable accuracy (Fig. 5). For the two end members values of 8.12 Å and 8.40 Å for SO_4- and CrO_4-AFm respectively were determined. Fig. 5 shows the two values for each sample except for Cr0.1 indicating the peak splitting.

The peak shifts observed in the XRD analysis show the formation of a solid solution between SO_4-and CrO_4-AFm, the peak splitting at $Crx \geq 0.2$ the existence of a miscibility gap. The lower boundary of the gap lies between 0.1<Crx>0.2, thus a value of 0.15 was estimated. Since no samples between 0.6<Crx>1 have been measured, an exact upper miscibility boundary cannot be set. Due to this lack of data, the most simple model, i.e. the presence of a regular solid solution, is assumed corresponding to a symmetric miscibility gap between $0.15 \leq Crx \leq 0.85$ (Fig. 5). Additional investigations would be needed to verify or reject this upper limit of the miscibility gap.

3.2. Solution analysis and thermodynamic modeling

Measured ion concentrations in solution show that with increasing Crx of the sample higher concentrations are present in solution. This is expected since pure SO_4-AFm has a lower solubility than CrO_4-AFm. Since traces of SO_4-ettringites were observed in samples with higher Crx content small shifts in the determined bulk concentrations occur for AFm phases. However, since no ettringite was observed in the XRD pattern, the amount of ettringite must be <1 weight%. Additionally, the presence of a secondary phase does not disturb solubility calculations as long as thermodynamic equilibrium has reached.

3.2.1. Solubility product of pure CrO_4- and SO_4-AFm

Based on measured ion concentrations from the pH dependent precipitation experiments, modeled ion activities, denoted by { },

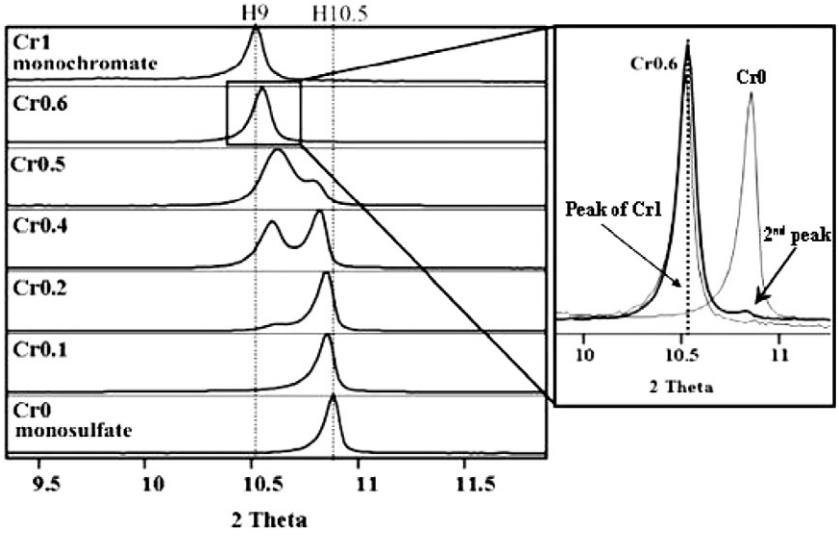

Fig. 4. Mixture samples between monochromate (Cr1) and monosulphate (Cr0) were measured at a relative humidity ≈30%. While Cr1 belonged to a hydration state of 9 (H9, corresponding to PDF 00-042-0063) monosulfate corresponds to a hydration state of 10.5 according to Pöllmann [29] and 10 after Dosch [34]. Except sample Cr0.1 where only one slightly shifted peak was observed, all other mixtures showed a small shift and peak splitting. The zoomed picture of sample Cr0.6 reveals as well a second peak - peak splitting.

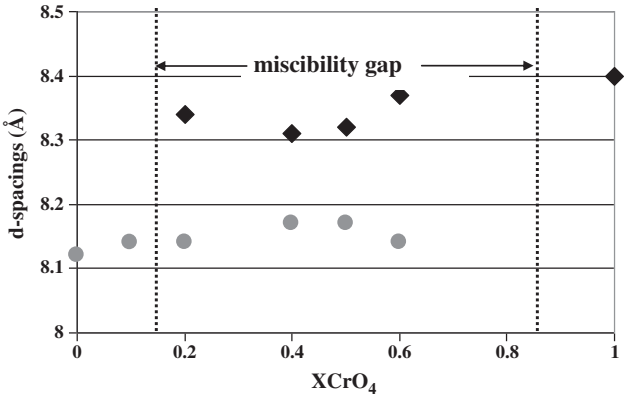

Fig. 5. Observed d-spacings of the mixture samples including pure monosulfate (Crx = 0; grey circles) and monochromate (Crx = 1; black diamonds). The black dotted lines indicate a miscibility gap between 0.15 ≤ Crx ≤ 0.85.

were used to calculate the solubility products (logK) of CrO_4-AFm according to Eq. (3):

$$\log K_{CrO_4-AFm} = 4\log\left\{Ca^{2+}\right\} + 2\log\{Al(OH)_4^-\} + \log\left\{CrO_4^{2-}\right\} + 4\log\{OH^-\} + 6\log\{H_2O\} \quad (3)$$

A mean log $K_{CrO4\text{-}AFm} = -28.4 \pm 0.7$ was determined (Fig. 6). No trend of the CrO_4-AFm solubility product with pH was observed. This value is somewhat lower than the published value of Perkins [7] with a log $K_{CrO4\text{-}AFm} = -30.4 \pm 0.3$. Recalculation of the data using the published concentrations of Perkins and Palmers [7,35] gave a log $K_{CrO4\text{-}AFm} = -30.0 \pm 0.5$. The solubilities measured by Zhang [10] gave log $K_{CrO4\text{-}AFm} = -29.4 \pm 0.3$.

The solubility product of pure SO_4-AFm was determined according to Eq. (3) (with SO_4 instead of CrO_4) resulting in a log $K_{SO4\text{-}AFm} = -29.7 \pm 0.4$. This corresponds well to the log $K_{SO4\text{-}AFm} = -29.3$ published by Matschei [36].

3.2.2. Monosulfate-monochromate solid solutions

Solubility data of the binary solid solution system are plotted in a diagram illustrating the evolution of Lippmann's total solubility product $\sum\prod$ of the solid phases (Fig. 7) [37,38]. The total solubility product ($\sum\Pi$) of solid solutions equals the sum of the partial solubility products (Eqs. (4) and (5)) of each end member, if the system has reached thermodynamic equilibrium. Adding up the left side of Eqs. (4) and (5) results in Eqs. (6) and (7) is the sum of the right side of Eqs. (4) and (5) leading to the following definitions of the total solubility products $\sum\Pi$.

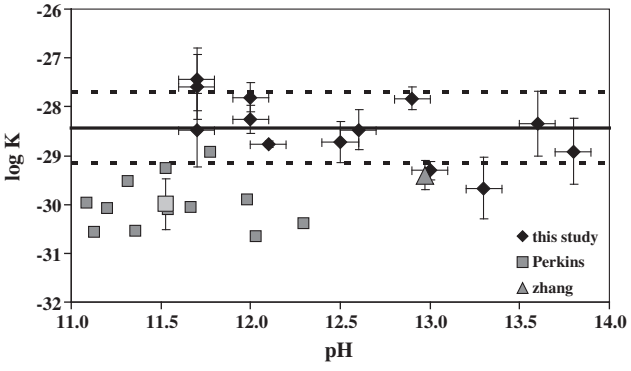

Fig. 6. Solubility products of monochromate determined from precipitation experiments at 25 °C between the pH range 11 and 14 resulted in a mean of logK −28.4 +/−0.7 at I = 0. Solubility products recalculated from the data given by Perkins and Palmer [7,35] and Zhang [10] have a lower solubility.

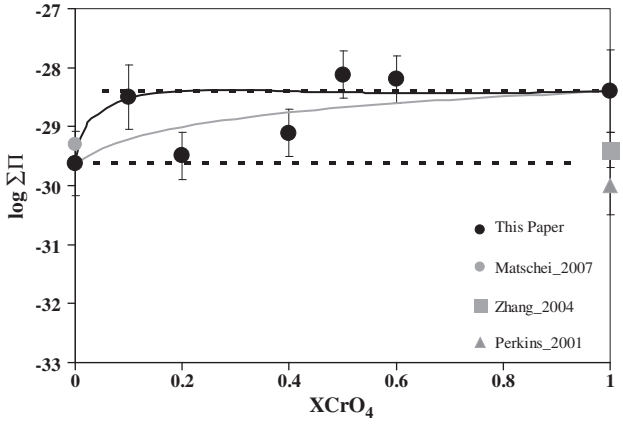

Fig. 7. The variation of the solubility product of SO_4- and CrO_4-AFm as well as the total solubility products (this paper) of mixed phases were determined at 25 °C and I = 0. The calculated curves indicate no solid solution formation (black dotted lines), ideal solid solutions (light grey line) and solid solution including a miscibility gap between 0.15 ≤ Crx ≤ 0.85 (black line). Solubility products of published pure SO_4- and CrO_4-AFm end-members are given.

$$K_{SO4-AFm}\cdot X_{SO4-AFm}\cdot\gamma_{SO4-AFm} = \left\{Ca^{2+}\right\}^4\cdot\left\{Al(OH)_4^-\right\}^2\cdot\left\{SO_4^{2-}\right\}\cdot\left\{OH^-\right\}^4\cdot\left\{H_2O\right\}^6 \quad (4)$$

$$K_{CrO4-AFm}\cdot X_{CrO4-AFm}\cdot\gamma_{CrO4-AFm} = \left\{Ca^{2+}\right\}^4\cdot\left\{Al(OH)_4^-\right\}^2\cdot\left\{CrO_4^{2-}\right\}\cdot\left\{OH^-\right\}^4\cdot\left\{H_2O\right\}^6 \quad (5)$$

$$\Sigma\Pi = K_{CrO4-AFm}\cdot X_{CrO4-AFm}\cdot\gamma_{CrO4-AFm} + K_{SO4-AFm}\cdot X_{SO4-AFm}\cdot\gamma_{SO4-AFm} \quad (6)$$

$$\Sigma\Pi = \left\{Ca^{2+}\right\}^4\cdot\left\{Al(OH)_4^-\right\}^2\cdot\left[\left\{CrO_4^{2-}\right\} + \left\{SO_4^{2-}\right\}\right]\cdot\left\{OH^-\right\}^4\cdot\left\{H_2O\right\}^6 \quad (7)$$

The waved brackets indicate ion activites, $K_{CrO4\text{-}AFm}$ and $K_{SO4\text{-}AFm}$ represent the solubility products of pure CrO_4- and pure SO_4-AFm, $X_{CrO4\text{-}AFm,\ SO4\text{-}AFm}$ are the chromate and sulfate mole fractions of the solid solution ($X_{CrO4\text{-}AFm} + X_{SO4\text{-}AFm} = 1$) and $\gamma_{CrO4\text{-}AFm,}$ $\gamma_{SO4\text{-}AFm}$ are the solid activity coefficient (with $\gamma = 1$ for ideal solid solutions). Solid activity coefficients are needed since the solid phase composition in a solid solution system changes according to variations in solution composition. The solid activity in a regular solid solution is no longer 1 as it is per definition for pure solids and in ideal solid solutions [23]. The solid activity coefficients can be expressed by the Guggenheim expansion series modified by Redlich and Kister expressions (Eqs. (8) and (9)) [39].

$$\ln\gamma_{CrO4-AFm} = X_{SO_4-AFm}^2\left[a_0 - a_1\left(3X_{CrO_4-AFm} - X_{SO_4-AFm}\right) + a_2(\ldots)\right] \quad (8)$$

$$\ln\gamma_{SO4-AFm} = X_{CrO_4-AFm}^2\left[a_0 - a_1\left(3X_{SO_4-AFm} - X_{CrO_4-AFm}\right) + a_2(\ldots)\right] \quad (9)$$

A regular solid solution series (with a symmetric miscibility gap) only needs one Guggenheim fitting parameter (a_0) which was determined by the MBSSAS code [40] based on the observed miscibility gap between 0.15 < Crx > 0.85. A value of $a_0 = 2.43$ resulted and was used to calculate the SO_4- and CrO_4-AFm end member activity coefficients.

Calculated total solubility products are illustrated in Fig. 7 (black points). Three different calculation models were compared to the experimentally determined points of log$\sum\Pi$. The first model does not

Table 3
CrO_4-AFm solubility (at I = 0) was determined by precipitation experiments between pH 11 and 14. Measured ion concentrations are listed.

Sample_pH	KOH (mM)	Ca (mmol/l)	Al (mmol/l)	Cr (mmol/l)	logK CrO_4-Afm
Cr1_14	1000	0.4	2.9	5.1	−28.5
Cr1_14	1000	0.4	3.2	4.7	−28.6
Cr1_14	1000	0.3	1.7	4.8	−29.7
Cr1_13.75	560	0.5	3.2	1.5	−28.5
Cr1_13.75	560	0.7	1.3	7.4	−28.2
Cr1_13.75	560	0.4	1.2	5.5	−29.5
Cr1_13.5	320	0.3	2.5	1.2	−29.7
Cr1_13.5	320	0.9	0.6	2.6	−28.8
Cr1_13.25	180	3.0	0.03	6.9	−29.3
Cr1_13.25	180	3.1	0.04	5.2	−29.0
Cr1_13	100	6.7	0.1	0.6	−27.8
Cr1_13	100	0.1	2.9	0.3	−28.1
Cr1_12.75	60	3.9	0.1	3.2	−28.5
Cr1_12.5	30	10.1	0.02	2.2	−28.7
Cr1_12.5	30	5.4	0.1	0.3	−29.3
Cr1_12.25	20	3.4	1.7	0.03	−28.7
Cr1_12.25	20	3.5	1.6	0.03	−28.8
Cr1_12.25	20	3.3	0.6	0.2	−28.8
Cr1_12	10	4.7	1.1	0.1	−28.4
Cr1_12	10	4.3	1.4	0.3	−27.9
Cr1_12	10	4.3	1.9	0.1	−28.5
Cr1_11.75	6	8.1	0.4	3.8	−27.8
Cr1_11.5	3	6.7	1.6	0.1	−27.7
Cr1_11.5	3	7.9	0.2	2.8	−28.5
Cr1_11.5	3	11.5	0.04	6.0	−29.2
Cr1_11.25	2	8.5	2.8	0.01	−28.0
Cr1_11.25	2	6.6	1.5	0.3	−27.6
Cr1_11.25	2	8.0	2.6	0.4	−26.7
Cr1_11	1	6.6	2.1	1.7	−27.4
Cr1_11	1	7.3	2.1	1.9	−27.1
Cr1_11	1	6.4	1.9	0.1	−28.3
Average					−28.4
stand. dev.					0.7

consider any solid solution formation, but assumes the presence of two solids. This means for the solubility products to be constant as indicated by the two doted lines at −29.6 for SO_4-AFm and −28.4 for pure CrO_4-AFm. Secondly, an ideal solid solution model was used, illustrated as by the grey line in Fig. 7. An ideal solid solution model (activity coefficient = 1) could have been used if no peak splitting and thus no miscibility gap would have been observed. The third and most realistic solid solution model included a miscibility gap, 0.15<Crx>0.85 (black line). However, based on the determined $\sum\Pi$, it cannot be decided whether and which kind of solid solution is present due to the relatively large error associated with the total solubility products (Fig. 7) and due to the small difference between the solubility products of pure SO_4- and CrO_4-AFm phases.

The presence of a solid solution with a miscibility gap is concluded from the peak shifts observed in the XRD patterns and from the observation that the solubility products of the SO_4- and CrO_4-AFm end-members (see the last two columns in Table 4) vary systematically with increasing sulfate content.

Table 4
Measured ion concentrations of the solid solution series are listed together with calculated total solubility products and solubility products of pure CrO_4- and SO_4-AFm (at I = 0). All prepared in 0.001 M KOH solution.

sample Crx	pH	Ca (mmol/l)	Al (mmol/l)	SO_4 (mmol/l)	CrO_4 (mmol/l)	log∑Π	*logK CrO_4-AFm*	*logK SO_4-AFm*
Cr1		see Table 3					−28.4	
Cr0.6_1	12.0	6.5	2.0	0.022	0.062	−28.0	*−28.2*	*−28.5*
Cr0.6_2	12.0	6.4	2.6	0.018	0.022	−28.2	*−28.6*	*−28.5*
Cr0.6_3	11.6	6.2	2.2	0.018	0.023	−28.4	*−28.7*	*−28.6*
Cr0.5_1	11.9	5.7	2.7	0.114	0.029	−27.9	*−28.8*	*−28.0*
Cr0.5_2	11.9	5.7	2.7	0.084	0.018	−28.1	*−29.0*	*−28.2*
Cr0.5_3	11.9	6.0	2.7	0.023	0.021	−28.3	*−28.8*	*−28.5*
Cr0.4_1	11.9	5.3	1.9	0.015	0.007	−29.1	*−29.6*	*−29.3*
Cr0.4_2	11.9	5.3	2.5	0.014	0.005	−29.0	*−29.5*	*−29.2*
Cr0.4_3	11.9	5.0	2.1	0.014	0.008	−29.2	*−29.7*	*−29.4*
Cr0.2_1	11.8	4.8	2.2	0.013	0.003	−29.5	*−30.4*	*−29.5*
Cr0.2_2	11.8	4.7	2.0	0.017	0.005	−29.5	*−30.2*	*−29.5*
Cr0.2_3	11.9	4.7	2.0	0.012	0.003	−29.5	*−30.3*	*−29.6*
Cr0.1_1	11.9	4.9	1.8	0.034	0.004	−29.1	*−30.2*	*−29.2*
Cr0.1_2	11.9	5.3	2.3	0.140	0.005	−28.2	*−29.9*	*−28.3*
Cr0.1_3	11.9	5.3	2.0	0.223	0.011	−28.1	*−29.6*	*−28.1*
Cr0_1	11.9	5.0	1.6	0.017				−29.4
Cr0_2	11.9	4.9	0.9	0.014				−29.6
Cr0_3	11.9	4.6	1.6	0.013				−29.9

4. Conclusion

In this study the solid solution series between SO_4- and CrO_4-AFm was investigated. The solubility product of pure CrO_4-AFm was determined at different pH values from precipitation experiments resulting in a $\log K_{CrO4\text{-}AFm} = -28.4 \pm 0.7$. The solubility product of the other end member SO_4-AFm was found to be $\log K_{SO4\text{-}AFm} = -29.7 \pm 0.4$. In experiments, where both CrO_4 and SO_4 have been present, peak shifts in the XRD diffractograms and varying solubility products of CrO_4-AFm and SO_4-AFm have been observed, indicating the formation of a solid solution. Based on the results a solid solution including a tentative miscibility gap between $0.15 < Crx < 0.85$ is proposed.

This study shows that the investigation of SO_4- and CrO_4-AFm solid solutions is complex and that the combination of different techniques is needed for the investigation and additional experiments would be needed to support the results presented here.

Acknowledgments

The financial support (Grant 200021-108057/1) of the Swiss National Foundation (SNF) is gratefully acknowledged. The authors would like to thank Hermann Mönch for his help during laboratory work. The authors would like to thank the two anonymous reviewers who improved the manuscript with their comments.

References

[1] A. Kindness, A. Macias, F.P. Glasser, Immobilization of chromium in cement matrices, Waste Manag. 14 (1) (1994) 3–11.
[2] D. Stephan, et al., High intakes of Cr, Ni, and Zn in clinker: Part I. Influence on burning process and formation of phases, Cem. Concr. Res. 29 (12) (1999) 1949–1957.
[3] S. Langard, M. Costa, eds. Chromium. Handbook on the Toxicology of Metals, ed. G. Nordberg, et al. 2007, Academic Press, Inc. 1024.
[4] J.O. Nriagu, E. Nieboer, eds. Chromium in the natural and human environments. 1 ed. Advances in Environmental Science and Technology, ed. J.O. Nriagu. Vol. 20. 1988, John Wiley & Sons, Inc. 571.
[5] M. Chrysochoou, D. Dermatas, Evaluation of ettringite and hydrocalumite formation for heavy metal immobilization: Literature review and experimental study, J. Hazard. Mater. 136 (1) (2006) 20–33.
[6] C.D. Palmer, Precipitates in a Cr(VI)-contaminated concrete, Environ. Sci. Technol. 34 (19) (2000) 4185–4192.
[7] R.B. Perkins, C.D. Palmer, Solubility of chromate hydrocalumite ($3CaO \cdot Al_2O_3 \cdot CaCrO_4 \cdot nH_2O$) 5-75°C, Cem. Concr. Res. 31 (7) (2001) 983–992.
[8] R.B. Perkins, C.D. Palmer, Solubility of ettringite ($Ca_6[Al(OH)_6]_2(SO_4)_3 \cdot 26H_2O$) at 5-75°C, Geochim. Cosmochim. Acta 63 (13–14) (1999) 1969–1980.
[9] T.C. Waddington, H.J.E.a.A.G. Sharpe, Lattice Energies and their Significance in Inorganic Chemistry, Advances in Inorganic Chemistry, Academic Press, 1959, pp. 157–221.
[10] M. Zhang, Incorporation of oxyanionic B, Cr, Mo and Se into hydrocalumite and ettringite: application to cementitous systems, Ph.D. Dissertation, in Earth Science. University of Waterloo Ontario, Canada, 2000.
[11] S.M. Leisinger, et al., Solid solutions between CrO_4- and SO_4-ettringite $Ca_6(Al(OH)_6)_2[(CrO_4)_x(SO_4)_{1-x}]_3{*}26\ H_2O$, Environ. Sci. Technol. 44 (23) (2010) 8983–8988.
[12] R. Allmann, Refinement of the hybrid layer structure$[Ca_2Al(OH)_6]^+[1/2\ SO_4{*}2H_2O]$, Neues Jahrb. Mineral. Monatsh. (1977) 136–144.
[13] R. Segni, Caractérisation structurale, propriétés d'échanges et stabilité de matériaux de type hydrocalumite $[Ca_2M(OH)_6]^+[X^{n1/n}{*}xH_2O]^-$ avec M=Al, Fe et Sc et X= SO_4, CrO_4, V_2O_7 et SiO_3., PhD Thesis, in Physique des Matériaux. Université Blaise Pascal: Clermon-Ferrand, France, 2005.
[14] J.-P. Rapin, Synthèse et etude cristallochimique de quelques aluminates et ferrites calciques hydrates de formule [Ca2M(OH)6]+, [X, nH2O]- with X = Cl, Br, I, ClO4, 1/2CrO4 and 1/2SO4 and M = Al and Fe, PhD Thesis, in Faculté de Sciences. Université Henri Poincaré: Nancy, France, 2001.
[15] R. Segni, et al., Hydrocalumite- type materials: 1. Interest in hazardous waste immobilization, J. Phys. Chem. Solids 67 (2006) 1037–1042.
[16] M. Francois, G. Renaudin, O. Evrard, A cementitous compound with composition 3CaO*Al2O3*CaCO3*11H2O, Acta Crystallogr. C54 (1998) 1214–1217.
[17] G. Renaudin, M. Francois, The lamellar double-hydroxide (LDH) compound with composition 3CaO*Al2O3*Ca(NO3)2*10H2O, Acta Crystallogr. C55 (1999) 835–838.
[18] T. Matschei, B. Lothenbach, F.P. Glasser, Thermodynamic properties of Portland cement hydrates in the system CaO-Al2O3-SiO2-CaSO4-CaCO3-H2O, Cem. Concr. Res. 37 (10) (2007) 1379–1410.
[19] A. Meshba, et al., Crystal structures and phase transition of cementitous bi-anionic AFm- (Cl^-, CO_3^{2-}) compounds, J. Am. Ceram. Soc. 94 (2011) 261–268.
[20] A. Meshba, et al., A new investigation of the Cl–CO32- substitution in AFm phases, J. Am. Ceram. Soc. 94 (2011) 1901–1910.
[21] A. Meshba, et al., Crystal structures of Kuzel's salt $3CaO\ Al_2O_3\ 1/2CaSO_4\ 1/2CaCl_2\ 11H_2O$ determined by synchrotron powder diffraction, Cem. Concr. Res. 41 (2011) 504–509.
[22] M. Atkins, F.P. Glasser, A. Kindness, Cement hydrate phases. Solubility at 25°C, Cem. Concr. Res. 22 (2–3) (1992) 241–246.
[23] M. Prieto, Thermodynamics of solid solution-aqueous solution systems, in: E.H. Oelkers, J. Schott (Eds.), Thermodynamics and Kinetics of Water-Rock Interaction, Mineralogical Society of America and Geochemical Society, 2009, pp. 47–85.
[24] A. Le Bail, Monte Carlo indexing with McMaille, Powder Diffr. 19 (3) (2004) 249–254.
[25] W. Feitknecht, H.W. Buser, Ueber den Bau der plaettchenfoermigen Calcium-Aluminiumhydroxysalze, Helv. Chim. Acta 34 (1951) 128–142.
[26] J. Goeske, U. König, H. Pöllmann, Kinetical investigations on lamellar calcium-aluminate chromate hydrates with high speed detector, Mater. Sci. Forum 43–44 (2004) 299–302.
[27] D.A. Kulik, U. Berner, E. Curti, Modelling chemical equilibrium partitioning with the GEMS-PSI code, PSI Scientific Report, PSI, Villigen, 2003, pp. 109–122.
[28] W. Hummel, et al., Nagra/PSI Chemical Thermodynamic Data Base 01/01, Universal Publishers/uPUBLISH.com, Parkland, Florida, USA, 2002.
[29] Poellmann, H., Die Kristallchemie der Neubildungen bei Einwirkung von Schadstoffen auf hydraulische Bindemittel, Ph.D. Dissertation, in Naturwissenschaftliche Fakultät. Friedrich-Alexander-Universität: Erlangen-Nürnberg. 1984
[30] H. Poellmann, H.J. Kuzel, S. Auer, ICDD Grant-in-Aid: Calcium aluminum chromium oxide hydrate 00-042-0063 in Mineralogical Institute, University of Erlangen, Erlangen, 1990.
[31] J. Goske, et al., ICDD Grant-in-aid: Calcium aluminum oxide chromium hydrate, Martin-Luther-University, Halle, 2001.
[32] H. Poellmann, S. Auer, ICDD Grant-in-aid: Calcium aluminum chromium oxide hydrate 00-041-0478, Mineralogica Institute, University of Erlangen, Erlangen, 1990.
[33] R.D. Shannon, Revised effective ionic radii and systematic studies of interatomic distances in halides and chalcogenides, Acta Crystallogr. A32 (1976) 751.
[34] Dosch, W. and H. Zur Strassen, Untersuchungen in den Alkali enthaltenen Systemen, gebildet aus den Komponenten CaO, Al2O3, Fe2O3, SiO2, SO3, Na2O, K2O H2O, Dissertation. University of Mainz: Mainz (GER). 1962
[35] Perkins, R.B., The solubility and thermodynamic properties of ettringite, its chromium analogs and calcium aluminum monochromate, Ph.D. Dissertation, in Environmental science and resources. Portland State University: Portland, USA. 2000
[36] T. Matschei, B. Lothenbach, F.P. Glasser, The AFm phase in Portland cement, Cem. Concr. Res. 37 (2) (2007) 118–130.
[37] F. Lippmann, Phase diagrams depicting aqueous solubility of binary mineral systems, Neues Jahrb. Mineral. Abh. 139 (1) (1980) 1–25.
[38] P.D. Glynn, E.J. Reardon, Solid-Solution Aqueous-Solution Equilibria - Thermodynamic theory and representation, Am. J. Sci. 290 (2) (1990) 164–201.
[39] O. Redlich, A.T. Kister, Algebraic representation of the thermodynamic properties and the classification of solutions, Ind. Eng. Chem. 40 (1948) 345–348.
[40] P.D. Glynn, MBSSAS: A code for the computation of Margules parameters and equilibrium relations in binary solid-solution aqueous-solution systems, Comput. Geosci. 17 (7) (1991) 907–966.
[41] J.D. Allison, D.S. Brown, K.J. Novo-Gradac, MINTEQA2/PRODEFA2, a geochemical assessment model for environmental systems: version 3.0, U.S.E.P. Agency, Editor. 1990.
[42] J.W. Ball, D.K. Nordstrom, Critical evaluation and selection of standard state thermodynamic properties for chromium metal and its aqueous ions, hydrolysis species, oxides, and hydroxides, J. Chem. Eng. Data 43 (6) (1998) 895–918.
[43] R.B. Perkins, C.D. Palmer, Solubility of $Ca_6[Al(OH)_6]_2(CrO_4)_3 \cdot 26H_2O$, the chromate analog of ettringite; 5-75°C, Appl. Geochem. 15 (8) (2000) 1203–1218.
[44] Y.M. Lee, C.L. Nassaralla, Standard free energy of formation of calcium chromate, Mater. Sci. Eng. A 437 (2) (2006) 334–339.